TORC1-dependent control of fission yeast cohesin

Dorian Besson, Sabine Vaur, Stéphanie Vazquez, Sylvie Tournier, Yannick Gachet, Adrien Birot, Stéphane Claverol, Adèle Marston, Anastasios Damdimopoulos, Karl Ekwall, et al.

TORC1-dependent control of fission yeast cohesin

Dorian Besson[1*], Sabine Vaur[1*], Stéphanie Vazquez[1], Sylvie Tournier[2], Yannick Gachet[2], Adrien Birot[1], Stéphane Claverol[3], Adèle Marston[4], Anastasios Damdimopoulos[5], Karl Ekwall[5] and Jean-Paul Javerzat[1§]

[1] CNRS, Université de Bordeaux - Institut de Biochimie et Génétique Cellulaires, UMR5095 - 33077 Bordeaux cedex, France

[2]MCD, Centre de Biologie Intégrative, Université de Toulouse, CNRS, UPS, Toulouse Cedex, France

[3]Univ. Bordeaux, Bordeaux Proteome, Bordeaux, France.

[4]The Wellcome Centre for Cell Biology, Institute of Cell Biology, University of Edinburgh, Edinburgh, EH9 3BF, UK

[5]Department of Biosciences and Nutrition, Karolinska Institutet, Huddinge, SE-141 83 Stockholm, Sweden.

*Equal contribution

[§]Correspondence to: JPaul.Javerzat@ibgc.cnrs.fr

ABSTRACT

The Target of Rapamycin Complex 1 (TORC1) integrates cellular cues and adapts cell growth and metabolism through substrate-specific phosphorylation. A genetic screen for suppressors of a conditional mutant of the cohesin loader Mis4 identified hypomorphic mutants of TORC1. Downregulation of TORC1 enhanced the binding of cohesin and its loader to their regular sites on chromosomes. In the context of impaired cohesin loading, TORC1 downregulation rescued chromosome segregation whereas upregulation had the opposite effect, suggesting environmental cues impinge on the robustness of chromosome segregation. TORC1 co-purified with cohesin from cellular extracts and the phosphorylation level of specific residues on Mis4 and cohesin were reduced in TORC1 mutants. Cohesin mutations mimicking the non-phosphorylated state mirrored the effects of TORC1 downregulation. Challenging cells with various conditions revealed that Mis4 and TORC1 regulate a common set of genes involved in the response to environmental changes. These genes are preferentially located far from centromeres and close to telomeres. We propose that cohesin is an effector of TORC1, orchestrating alterations in chromosome structure that facilitate cellular adaptation to environmental changes.

INTRODUCTION

The cohesin complex is a pivotal player in genome structure and function. Its activity is critical for a variety of biological processes, including sister chromatid cohesion, nuclear division, DNA replication and repair, and gene expression. Cohesin is an ATP-powered molecular machine that is capable of capturing DNA. Intra-chromosomal DNA capture folds the interphase genome into loops, which contributes to gene regulation, particularly during development and cell fate decisions. Conversely, DNA capture in trans provides cohesion between sister chromatids, which is essential for chromosome segregation and repair (Zheng & Xie, 2019; Davidson & Peters, 2021; Oldenkamp & Rowland, 2022). The core cohesin complex consists of two Structural Maintenance of Chromosome proteins, Smc1 and Smc3 (Psm1 and Psm3 in the fission yeast *Schizosaccharomyces pombe*) whose ATPase heads are bridged by a kleisin subunit (Rad21/Scc1) to which a fourth subunit (hSTAG1-2, spPsc3, scScc3) binds. DNA capture by cohesin requires the so-called loading complex NIPBL/MAU2 (spMis4/Ssl3, scScc2/Scc4) which binds to cohesin and DNA. Inactivation of the cohesin loading machinery before S phase results in the failure of sister-chromatid cohesion establishment and aberrant chromosome segregation during the ensuing mitosis (Furuya *et al*, 1998; Ciosk *et al*, 2000; Bernard *et al*, 2006). Similarly, DNA loop extrusion is dependent on the NIPBL-Cohesin holocomplex (Davidson *et al*, 2019). Chromatin loops are dynamic structures that form and break on a time-scale of minutes. In human, the DNA binding factor CTCF appears to delineate loop domains, often referred to as topologically associated domains (TADs). Dynamically extruding cohesin complexes are thought to facilitate enhancer-promoter scanning *in cis*. TAD boundaries (insulation) appear regulated as the strengths of CTCF-anchored loop domains are enhanced when mouse embryonic stem cells exit pluripotency. Consistently, mutations in the genes encoding CTCF and cohesin components are linked to human diseases and developmental abnormalities (Zheng & Xie, 2019; Davidson & Peters, 2021; Oldenkamp & Rowland, 2022). The remodelling of genome architecture appears particularly important for appropriate gene expression during cell fate decisions, suggesting that signalling pathways should convey cellular cues to cohesin. In this context, a recent screen in mammalian cells identified a set of kinases that alter chromosome folding when inactivated (Park *et al*, 2023).

Here we report a link between fission yeast cohesin, its loader Mis4 and the Target of Rapamycin Complex 1 (TORC1). TORC1 is a master regulator of cell growth and metabolism, highly conserved in eukaryotes. The kinase activity of TORC1 is stimulated by a variety of intra- and extracellular signals,

including nutrients, growth factors, hormones and cellular energy levels. Once activated, TORC1 promotes cell growth and metabolism through the phosphorylation of multiple effectors (González & Hall, 2017; Otsubo *et al*, 2017). In mammalian species, growth factors and cellular energy stimulate the activity of mTORC1 through the Rheb GTPase, and the inhibition of the tuberous sclerosis complex (TSC), which functions as a GTPase-activating protein for Rheb. In response to amino acid availability, mTORC1 is activated via RAG GTPases in a TSC-independent manner. Under nutrient-rich conditions, TORC1 promotes anabolic processes, such as protein, nucleotide, and lipid synthesis, while inhibiting catabolic processes, such as autophagy.

In fission yeast, Tor2 provides the catalytic activity of TORC1, while Mip1, the Raptor equivalent, participates in substrate recognition (Morozumi *et al*, 2021). The complex contains three additional subunits, the mLST8 orthologue Wat1/Pop3, Toc1 and Tco89 (Hayashi *et al*, 2007). TORC1 plays a crucial role in switching between cell proliferation and differentiation by sensing nitrogen source. When deprived of nitrogen, fission yeast cells arrest in G1, mate and undergo meiosis. In the absence of a mating partner, G1 cells enter a G0, quiescent state. Like its mammalian counterpart, the Rheb GTPase Rhb1 is an essential activator of TORC1. Upon nitrogen deprivation, TORC1 activity is restrained by the Gtr1-Gtr2 GTPases, the TSC complex, and the Gcn2 kinase (van Slegtenhorst et al, 2004; Chia et al, 2017; Fukuda & Shiozaki, 2018; Fukuda et al, 2021). In conditions of abundant nutrients, TORC1 activity is high but nevertheless attenuated by the Gtr1-Gtr2 heterodimer, which is analogous to the mammalian RAG GTPases (Chia et al., 2017; Fukuda and Shiozaki, 2018). TORC1 is essential for cell growth, and loss of the TORC1 activity results in cell cycle arrest in G1. Rapamycin only partially inhibits TORC1 activity in *S. pombe* and does not inhibit growth (Otsubo *et al*, 2017).

The link between cohesin and TORC1 arose from a genetic screen for mutants able to suppress the thermosensitive growth (Ts) defect of *mis4-G1487D*, which is defective for cohesin loading and chromosome segregation at the restrictive temperature (Birot *et al*, 2020). In principle the screen had the potential to identify regulators of Mis4, with the rationale that loss of a negative regulator should upregulate residual Mis4^{G1487D} activity and restore growth at the restrictive temperature. In addition to a cyclin-dependent kinase (CDK) called Pef1, which acts as a negative regulator of Mis4 (Birot *et al*, 2020), several mutants of TORC1 were recovered. This study demonstrates that downregulation of TORC1 in fission yeast enhances cohesin binding to Cohesin-Associated Regions (CARs). In the context of impaired cohesin loading, downregulation of TORC1 rescued chromosome segregation, while upregulation had the opposite effect. TORC1 and cohesin co-purified from protein extracts, and the phosphorylation level of specific residues on cohesin and its loader was reduced in TORC1 mutants. Cohesin mutations mimicking the non-phosphorylated state had similar effects to TORC1 downregulation. Hence cohesin behaves as an effector of TOR signalling, opening the intriguing possibility that environmental cues could affect the robustness of chromosome segregation processes.

As TORC1 is known to direct transcriptional responses to environmental signals, we investigated the potential role of Mis4 in this pathway by analysing the transcriptome of *mis4-G1487D* cells in a variety of experimental situations designed to mimic changes that might occur in a natural environment. These include variations in the composition of the culture medium, temperature, time, and cell cycle phase. Remarkably, the genes affected differed widely from one condition to another, suggesting a defective adaptive response. Almost all the genes deregulated by *mis4-G1487D* were also deregulated by *mip1-R401G*, suggesting that cohesin and TORC1 act in the same pathway. These genes are preferentially located at the ends of chromosomes and are involved in the stress response and sexual differentiation.

Collectively, the data presented here indicate that TORC1 controls the association of cohesin and its loader with chromosomes, regulating their functions in chromosome segregation during mitosis and in the transcriptional response to environmental changes.

RESULTS

A genetic screen for suppressors of *mis4-G1487D* identified components of TORC1

The G1487D substitution in the cohesin loader Mis4 renders the strain thermosensitive for growth (Ts, Figure 1A). At the restrictive temperature the amount of cohesin associated with chromosomes is reduced and cells exhibit defects in chromosome segregation during mitosis (Birot *et al*, 2020). To identify putative regulators of Mis4, we previously carried out a genetic screen for suppressors of the Ts phenotype of *mis4-G1487D* (Birot *et al*, 2020). One of the suppressors identified was Pef1, a CDK whose activity restrains cohesin binding to Cohesin Associated Regions (CARs). Besides *pef1*, the genetic screen identified three other genes: *tor2* (1 allele), *mip1* (5 alleles) and *caa1* (1 allele). The suppressive effect of the *caa1* mutant was modest (Fig.1, Supplement 1). On the other hand, *tor2* and *mip1* mutants clearly suppressed the Ts phenotype of *mis4-G1487D*, at a level similar to that conferred by the deletion of the *pef1* gene (Fig. 1A).

The *caa1* gene encodes an aspartate aminotransferase that is required for full activation of the TORC1 complex (Reidman *et al*, 2019). Tor2 and Mip1 are components of TORC1 ((Hayashi *et al*, 2007), Fig.1B). Both genes are essential for cell survival. The *tor2* allele recovered in our genetic screen bears a substitution in the kinase domain which affected colony growth suggesting that TORC1 activity is largely affected. The five Mip1/Raptor mutants did not show this phenotype, the growth being similar to that of a wild strain. Still they all show reduced phosphorylation of the S6-kinase Psk1 (Fig.1C), a well-known TORC1 substrate (Nakashima *et al*, 2012). Similarly, the *mip1-Y533A* mutant which is deficient for Psk1 binding and phosphorylation (Morozumi *et al*, 2021), suppressed the Ts phenotype of *mis4-G1487D* (Fig1C). In a similar manner, the pharmacological downregulation of TORC1 by rapamycin resulted in enhanced growth of *mis4-G1487D* at the restrictive temperature (Fig.1D). Other thermosensitive mutants of the cohesin pathway (*eso1-H17* and *rad21-K1*) were not rescued ruling out a general suppressing effect. Hence, the suppression of *mis4-G1487D* may stem from reduced TORC1 kinase activity. Conversely, the genetic upregulation of TORC1 exacerbated the Ts phenotype of *mis4*-G1487D. TORC1 activity upon nitrogen deprivation is restrained by the Gtr1-Gtr2 GTPases, the TSC complex, and the Gcn2 kinase. Among these, the Gtr1-Gtr2 GTPases dampen TORC1 even in nutrient replete conditions (Fig.1E, (van Slegtenhorst *et al*, 2004; Chia *et al*, 2017; Fukuda & Shiozaki, 2018; Fukuda *et al*, 2021)). The deletion of *gcn2* or *tsc2* was essentially neutral in terms of *mis4-G1487D* suppression, although the suppression by *mip1-R401G* was reduced in a *tsc2*-deleted background. Deletion of *iml1, gtr1* or the *gtr1-Q61L* allele (mimicking the GTP-bound inactive state of the Gtr1 GTPase, (Chia *et al*, 2017)) exacerbated the Ts phenotype of *mis4-G1487D* while mimicking the active GDP-bound form by using the *gtr1-16N* allele, (Chia *et al*, 2017)) was neutral. The deletion of *tor1*, encoding the catalytic subunit of the related complex TORC2 exacerbated the Ts phenotype of the *mis4* mutant (Fig1, Supplement 1). As TORC1 kinase activity is upregulated when *tor1* is deleted (Ikai *et al*, 2011), this observation is in line with the notion that *mis4-G1487D* is sensitive to hyperactive TORC1.

The above genetic analyses show that the Ts phenotype of the *mis4* mutant is dampened when TORC1 activity is down-regulated and exacerbated when TORC1 is up-regulated. Because *mip1* alleles barely affected growth on their own and were excellent *mis4* suppressors we focused our analyses on one of them, *mip1-R401G*. We found that *mip1-R401G* acted as suppressor in another genetic context of impaired cohesin loading. The acetyl-mimicking forms of Psm3 have been demonstrated

to impede the loading of cohesin (Murayama & Uhlmann, 2015; Hu *et al*, 2015; Birot *et al*, 2020). This phenotype is exacerbated by the deletion of *pph3*, encoding the catalytic subunit of PP4 and the double mutant strain is Ts for growth (Birot *et al*, 2020). The *mip1-R401G* mutant efficiently suppressed the Ts phenotype of *psm3-K105NK106N pph3*Δ (Fig.1F), indicating that the suppression is not restricted to *mis4-G1487D* but appears generally related to cohesin loading.

The occurrence of chromosome segregation defects in *mis4-G1487D* is modulated by TORC1

When *mis4-G1487D* cells were shifted to the restrictive temperature cell proliferation was reduced and viability dropped ~25 fold after 24 hours when compared to wild-type. The *mip1-R401G* mutation efficiently suppressed the proliferation and viability defects (Fig.2A). A hallmark of cohesin mutants is the occurrence of abnormal mitoses in which the spindle apparatus attempts to segregate un-cohesed sister chromatids. A single kinetochore is captured by microtubules emanating from opposite spindle poles (merotelic attachment) and moves back and forth on the anaphase spindle as a result of opposite forces (Pidoux *et al*, 2000; Gregan *et al*, 2011). Live cell analysis confirmed the occurrence of merotelic kinetochores in the *mis4* mutant (Fig.2 supplement 1). In fixed cells, a merotelically-attached chromatid appears as DAPI-stained material lagging on the anaphase spindle. Anaphases with lagging DNA were frequent for *mis4-G1487D* after one doubling of the cell population at the restrictive temperature and their occurrence was significantly reduced by *mip1-R401G* (Fig.2B). Merotelic kinetochores oppose spindle forces and reduce the rate of spindle elongation during anaphase. As the number of merotelic kinetochores increases the spindle elongation rate slows down and may even become negative resulting in spindle shrinkage (Courtheoux *et al*, 2009). The rate of spindle elongation was strongly affected in *mis4-G1487D* and spindle shrinkage events were frequent, indicative of a high level of merotely. Spindle shrinkage occurred in ~53% of anaphases in *mis4-G1487D* whereas it was reduced to ~21% in the *mip1-R401G* background (Fig.2C and Fig.2 supplement 2). Particularly striking was the observation of spindle shrinkage followed by asymmetric spindle displacement resulting in the generation of anucleate daughter cells after cytokinesis (Fig.2D). Nearly 80% of cells showed this phenotype in *mis4-G1487D* for the late time points whereas the frequency was reduced to ~20% in the presence of *mip1-R401G*. Altogether, these analyses indicate that the *mis4* mutant experienced numerous merotelic events during anaphase at the restrictive temperature, leading to asymmetric spindle shrinkage and the production of anucleate cells. The suppression of these phenotypes by *mip1-R401G* is consistent with a lower incidence of merotelic attachments. Although the effect was weaker, rapamycin also reduced the frequency of anaphases with lagging DNA (Fig.2E). This is consistent with the notion that the down-regulation of TORC1 reduced chromosome segregation defects of the *mis4* mutant. Physiologically TORC1 acts as a rheostat, its activity rising with nutrient availability. Consistently, the severity of the Ts phenotype and the frequency of lagging DNA were higher in the rich, complete medium YES than in the synthetic minimal medium EMM2 (Fig.2F). YES is a complex undefined medium containing numerous sources of nitrogen, whereas ammonia is the sole source of nitrogen in EMM2. The use of glutamate, a nitrogen source slightly poorer than ammonia (Davie *et al*, 2015) further reduced chromosome segregation defects (Fig2. Supplement 3). The artificial increase of TORC1 activity by *gtr1-Q61L* resulted in an elevated rate of anaphases with lagging DNA (Fig.2F). Altogether, these analyses show that TORC1 activity modulates the occurrence of chromosome segregation defects of *mis4-G1487D*.

Remarkably, the suppressor effect of the *mip1-R401G* mutation was not restricted to the *mis4* mutant. The frequency of anaphases with lagging DNA was efficiently reduced in the $psm3^{K105N\text{-}K106N}$ *pph3*Δ background (Fig.2G). As for *mis4-G1487D*, cohesin loading is impaired in this genetic setup

(Birot *et al*, 2020) but Mis4 is wild-type, suggesting the suppression may stem from an upregulation of the cohesin loading machinery.

Although the down-regulation of TORC1 reduced chromosome segregation defects, they were not fully suppressed suggesting that sister-chromatid cohesion was poorly restored. The monitoring of sister-chromatid cohesion at the *ade6* locus (Molnar *et al*, 2003) revealed a persistent defect and the level of Psm3 acetylation, a marker of sister-chromatid cohesion establishment, remained low. Likewise, rapamycin treatment did not improve Psm3 acetylation (Fig2 supplement 4). We suspect that sister-chromatid cohesion remained largely defective but improved enough to reach the critical threshold allowing cell proliferation.

Reduced TORC1 activity increased Mis4 and cohesin binding to Cohesin Associated Regions (CARs)

The cohesin loading complex performs its essential function during G1/S (Furuya *et al*, 1998; Ciosk *et al*, 2000; Bernard *et al*, 2006). The down-regulation of TORC1 may rescue *mis4-G1487D* by up-regulating its residual cohesin loading activity. To address this issue, cells were arrested at the end of the G1 phase by the use of the *cdc10-129* Ts mutation and cohesin binding to chromosomes monitored by Rad21 ChIP-qPCR at known CARs (Fig.3A). Cycling *S. pombe* cells are essentially in the G2 phase of the cell cycle (Carlson *et al*, 1999). When shifted at 36.5°C, *cdc10-129* cells progress through G2, M and arrest in G1. As reported previously, Rad21 binding to CARs was reduced in a *mis4-G1487D* background (Feytout *et al*, 2011; Vaur *et al*, 2012; Birot *et al*, 2020). The *mip1-R401G* mutation efficiently restored cohesin binding to near wild-type levels (Fig. 3B). A similar effect was observed in the $psm3^{K105N\text{-}K106N}$ *pph3*Δ background (Fig.3 supplement 1) indicating that *mip1-R401G* restores cohesin loading in these two distinct genetic contexts. Importantly, a similar effect was observed in cells with a wild-type cohesin loading machinery. In an otherwise wild-type background, Mis4 and Rad21 binding to CARs were increased in *mip1-R401G* cells at most chromosomal sites examined (Fig.3C-D). Rapamycin treatment provoked a similar effect although less pronounced (Fig3 supplement 1). We conclude that TORC1 down-regulation increases cohesin abundance at CARs, presumably by stimulating cohesin loading.

TORC1 components co-purify with cohesin and its loader

To see whether TORC1 and cohesin may interact we affinity-purified Mis4 and Rad21 complexes and analysed associated proteins by label-free mass spectrometry (Fig.4A). To avoid cell cycle effects, extracts were prepared from G1 (*cdc10-129*) arrested cells. All TORC1 components co-purified with Mis4 and Rad21 and conversely, additional co-immunoprecipitation experiments showed that cohesin co-purified with TORC1 (Fig.4B-C). This observation suggests that Cohesin and its loader may be TORC1 substrates.

Reduced Mis4-S183 and Psm1-S1022 phosphorylation levels in *mip1* mutants

To see whether *mip1-R401G* may alter cohesin or Mis4 phosphorylation status, Mis4 and Rad21 complexes were purified from *mip1-R401G* and $mip1^{+}$ cells and triplicate samples analysed by label-free mass spectrometry. As before, protein extracts were prepared from G1-arrested cells to avoid cell cycle induced changes. A serine residue (S183) within the N terminal domain of Mis4 was less phosphorylated in *mip1-R401G* compared to wild-type. Likewise, Psm1-S1022 phosphorylation level was decreased (Fig.5A).

Antibodies were raised against the phosphorylated forms (Fig.5 supplement 1) and this confirmed that the levels of Mis4-S183p and Psm1-S1022p were reduced in *mip1-R401G* cells. A similar reduction was also apparent in the unrelated mutant *mip1-Y533A* (Fig. 5B and D).

Mis4-S183 and Psm1-S1022 may be direct TORC1 targets or the substrates for kinases downstream TORC1. Both phosphorylation sites adhere to the CDK consensus (S-T/P) but were not described as direct targets of Cdc2, the main fission yeast CDK (Swaffer *et al*, 2018). Label-free mass spectrometry indicated that Mis4-S183p was not dependent on the CDK Pef1 either (Fig. 5A supplement). However, Psm1-S1022 phosphorylation was strongly reduced in *pef1* deleted cells (Fig.5C-D supplement 1). The Pef1 CDK was reported as a positive regulator of TORC1 (Matsuda *et al*, 2020). Indeed, the phosphorylation level of the TORC1 substrate Psk1 was reduced in *pef1* deleted cells and the double mutant *pef1*Δ *mip1-R401G* grew very poorly (Fig.5F supplement 1). Pef1 may therefore activate TORC1 for the phosphorylation of Psm1. Conversely, Pef1 activity does not seem to depend on TORC1 as Rad21-T262p, which is a Pef1 substrate (Birot *et al*, 2020), was not affected by *mip1-R401G* (Fig. 5D supplement). The interplay between TORC1, Pef1 and possibly other kinases downstream of TORC1 remains to be elucidated. Whatever the mechanism, the above data show that TORC1 signalling affects the phosphorylation level of Mis4 and Psm1.

Mis4-S183 and Psm1-S1022 are relevant targets for the regulation of cohesin by TORC1

The above data suggest that TORC1 down-regulation may rescue *mis4-G1487D* through reduced phosphorylation of Mis4 and Psm1 to stimulate cohesin loading. To address this hypothesis we generated mutants mimicking the non-phosphorylated (S to A) or phosphorylated state (S to E/D). Non-phosphorylatable *mis4* and *psm1* mutants rescued *mis4-G1487D* growth and chromosome segregation defects while phospho-mimetics had the opposite effect (Figure 6A-C). Cohesin binding to CARs as assayed by ChIP tend to increase for the mutants mimicking the non-phosphorylated state and to decrease with the phospho-mimicking forms (Fig.6D). Likewise, non-phosphorylatable *mis4* and *psm1* mutants efficiently rescued growth and chromosome segregation defects in the *psm3*$^{K105N-K106N}$ *pph3*Δ background (Fig.6 supplement 1). ChIP analyses revealed that cohesin binding to CARs was clearly stimulated, consistent with an upregulation of the cohesin loading machinery when Mis4-S183 and Psm1-S1022 are not phosphorylated. Altogether these data argue that Mis4 and Psm1 are relevant downstream effectors for cohesin regulation by the TOR signalling pathway.

Mis4 and TORC1 control a common set of genes involved in the response to environmental changes

The link between TORC1 and cohesin suggested the possibility that cohesin controls the transcriptional response to environmental changes. To address this possibility we looked at the transcriptome by RNA-sequencing of wild-type, *mis4-G1487D* and *mip1-R401G* cells in various experimental conditions (Fig.7). These included cycling cells in the rich complete medium YES at 25°C (V25) and upon a temperature shift to 36.5°C for one doubling (V36.5) or arrested in G1 (*cdc10-129*) at this temperature (G1_36.5). We also looked upon nitrogen starvation by shifting actively cycling cells from the synthetic medium EMM2 to EMM2 deprived of a nitrogen source (EMM2-N). In this situation, TORC1 activity is restrained, cells arrest in G1 and either mate to enter the reproductive cycle (meiosis) or enter a G0, quiescent state. As no mating partner was available in our experiments, cells homogeneously arrested in G1 after nitrogen deprivation (Fig.7 supplement 1). RNA-sequencing was performed 24 hours after the shift to EMM2-N (T0-N). One half of the remaining culture was then shifted to 36.5°C for 4 days (T4D36.5) while the other half was kept at 25°C for 4 days (T4D25). The results are summarized in Figure 7 and the detailed gene lists are given in supplementary Table 1.

The first striking observation is the low number of genes whose expression was affected in *mis4-G1487D* versus wild-type in actively growing cells in rich medium (Fig.7A, V25, 12 genes), even after G1 arrest (G1_36.5, 27 genes) or one cell doubling (V36.5, 50 genes) at the restrictive temperature.

The number of differentially expressed genes increased upon nitrogen deprivation (T0-N, 118 genes, T4D25, 125 genes) even though 25°C is a permissive temperature for *mis4-G1487D*. A similar number of genes were misregulated in *mis4-G1487D* when nitrogen depleted cells were shifted to 36.5°C for 4 days (T4D36.5, 76 genes). These first observations indicate that the number of genes affected by *mis4-G1487D* is not increased by the shift to the non-permissive temperature. This may suggest that the defect in gene expression of *mis4-G1487D* is not conditional.

A second striking observation emerged when we compared the list of misregulated genes in the different experimental conditions. The graph in Fig.7B shows that there is little overlap between gene lists. For instance, 70% of the genes misregulated 24 hours after nitrogen depletion (T0-N) were specific to that condition and four days later (T4D25), 77% of the gene list were specific to that stage. Cells deprived of a nitrogen source first arrest in G1 and then progress into the quiescent state. Mis4 appears required for appropriate gene expression changes as cells enter and progress through quiescence. The other gene lists also showed a low level of overlap, further strengthening the idea that Mis4 is required for the regulation of gene sets involved in the response to specific changes in the environment.

In aggregate, 337 genes were misregulated in *mis4-G1487D* across all experiments. Strikingly, most of these (300/337) were also affected by *mip1-R401G* (Fig.7C). A strong overlap was also apparent with a published set of genes whose expression was upregulated in a *tor2* conditional mutant at the restrictive temperature (Fig. 7D, (Wei *et al*, 2021)). A significant overlap was also seen with genes up-regulated in G0 (Zahedi *et al*, 2023), suggesting Mis4 may participate in the proper establishment and/or maintenance of the quiescent state (Fig. 7E). Cell survival remains high in G0 in the *mis4* and *mip1* mutants (Fig.7 supplement 2-3) but upon refeeding a delay in G0 exit was noticeable (Fig.7 supplement 4). This phenotype was quite strong for *mip1-R401G* and much more subtle for the *mis4* mutant. Nevertheless, any delay in G0 exit may reduce the competitive fitness. The analysis of gene lists with AnGeLi (Bitton *et al*, 2015) indicated that *mis4*-regulated genes showed a strong localization bias towards chromosome ends, as previously reported (Dheur *et al*, 2011), an enrichment for “stress genes”, the response to nitrogen starvation and differentiation (meiosis). Genes encoding membrane transporters were significantly enriched, suggesting a role for Mis4 in cell homeostasis.

Overall, these data show that Mis4 and TORC1 control a common set of genes involved in the response to environmental changes.

DISCUSSION

The data presented in this work provide evidence for a regulation of cohesin by the TOR signalling pathway. This is, to the best of our knowledge, the first report to demonstrate such a relationship. Previously, a link had been established between the two pathways, but in the opposite direction. mTORC1 is indeed down-regulated in cells from patients with Roberts syndrome, caused by mutational alteration of the ESCO2 cohesin acetyl-transferase (Xu *et al*, 2013). The down-regulation of the cohesin loader NIPBL in breast cancer cells induced cell cycle arrest, apoptosis and autophagy through the caspase 3 and mTOR signalling pathways (Zhou *et al*, 2017). The first hint for a regulation of cohesin by the TOR pathway came from the observation in fission yeast that the growth of a conditional mutant of *mis4* was enhanced by rapamycin (Sajiki *et al*, 2018). In mammalian species, a fraction of mTOR controls nuclear processes, notably transcription (Zhao *et al*, 2024). Likewise, fission yeast TORC1 is involved in the regulation of facultative heterochromatin (Wei *et al*, 2021; Hirai *et al*, 2023) and transcriptional processes (Laribee & Weisman, 2020). The present work establishes a close link between cohesin and the TOR pathway, suggesting the exciting possibility that extracellular

signals could remodel the functional architecture of chromosomes during differentiation or adaptation processes.

Mis4 and Psm1 as downstream targets of TORC1

We present evidence showing that cohesin and TORC1 components co-purify from protein extracts and Mis4-S183 and Psm1-S1022 are less phosphorylated in *mip1* mutants. Non-phosphorylatable mutants recapitulated most of the effects of TORC1 down-regulation while mutants mimicking the phosphorylated state produced phenotypes similar to TORC1 hyper activation. Whether cohesin and Mis4 are substrates of TORC1 or other kinases regulated by TORC1 is currently unknown. Meanwhile, our work provides the first evidence that cohesin is a downstream effector of TORC1. Both phosphorylation events on Mis4 and Psm1 have been reported in the literature but their biological functions are unknown (Kettenbach *et al*, 2015; Swaffer *et al*, 2018; Tay *et al*, 2019; Halova *et al*, 2021). Mis4-S183 is located within an unstructured, flexible region connecting the Ssl3 interaction domain and the hook domain that provides Mis4 catalytic activity. It was proposed that phosphorylation at CDK sites within the unstructured linker may affect the flexibility of the complex and modulate its activity (Chao *et al*, 2015). Mis4-S183 and the CDK consensus are conserved in hNIPBL and the S1160 residue was found phosphorylated in a number of phosphoproteomic studies (Ruse *et al*, 2008; Dephoure *et al*, 2008; Pan *et al*, 2009; Mayya *et al*, 2009; Christensen *et al*, 2010; Rigbolt *et al*, 2011; Beli *et al*, 2012). Cryo-EM structures of cohesin bound to its loader and DNA revealed that the SMC coiled coils are folded around their elbow (Collier *et al*, 2020; Shi *et al*, 2020). The S1022 residue of Psm1 lies close to the "joint" region below the ATPase heads that the "hinge" domain contacts when cohesin in its folded conformation. Whether the phosphorylation of Psm1-S1022 affects the outcome of DNA transactions remain to be investigated.

TORC1 activity restrains cohesin binding to CARs

Reducing TORC1 activity by the *mip1-R401G* mutation or rapamycin treatment enhanced Cohesin binding to CARs. This was observed for two genetic contexts of sensitized cohesin loading and with a wild-type cohesin loading machinery. The most straightforward interpretation is that TORC1 restrains cohesin loading. A distinct possibly would be that TORC1 down-regulation promotes cohesin accumulation at CARs without *de novo* loading. It was proposed that CARs correspond to the borders of yeast TAD-like structures (Costantino *et al*, 2020). Increased abundance of cohesin at CARs may result from the accumulation of cohesin with loop extrusion activity at TAD boundaries. Considering that loop extrusion requires the NIPBL-Cohesin holocomplex (Davidson *et al*, 2019), it is interesting to note that Mis4 binding to CARs was similarly enhanced. TORC1 may also impinge on cohesin sliding by transcription-related processes (Lengronne *et al*, 2004; Schmidt *et al*, 2009) and / or influence cohesin accumulation through the phosphorylation of chromatin-bound proteins. Future work will aim at clarifying these issues.

TORC1 and chromosome segregation

Cells with a crippled cohesin loading machinery experience chromosome segregation defects during mitosis. We have shown here that the intensity of the defect is dependent on TORC1 activity. The most prominent defect is the merotelic attachment of kinetochores which, when left uncorrected, lead to aberrant chromosome segregation. Although the down-regulation of TORC1 reduced the frequency of aberrant anaphases, sister-chromatid cohesion was still largely impaired although cohesin binding to CARs in the *mis4* mutant was restored to near wild-type levels in cells arrested at the G1/S boundary. The increase in chromosome bound cohesin may have enhanced cohesion establishment during S-phase. Chromosome segregation defects were indeed reduced but sister-chromatid cohesion remained overall defective. Consistently, cohesin acetylation was not improved

by TORC1 down-regulation. The acetylation of Psm3, mediated by Eso1 in fission yeast, counteracts the cohesin releasing activity of Wapl and is thought to stabilize cohesin binding and cohesion (Feytout *et al*, 2011; Kagami *et al*, 2011; Vaur *et al*, 2012; Birot *et al*, 2017). However, deletion of the *wpl1* gene does not rescue the *mis4-G1487D* mutant and *S. pombe* cells can survive with non-detectable acetylation or in a context in which Psm3 cannot be acetylated (Feytout *et al*, 2011; Birot *et al*, 2020). The primary defect of *mis4-G1487D* may therefore stem from inability to generate sister-chromatid cohesion rather than its maintenance. *In vitro* assays have suggested that sister-chromatid capture by cohesin is a two-step process catalysed by Mis4 (Murayama *et al*, 2018). The down-regulation of TORC1 may increase the residual loading activity of Mis4 but second DNA capture may remain largely deficient, resulting in poor sister-chromatid cohesion. Increased cohesin binding at peri-centromeres may improve chromosome segregation through other routes. Cohesin organizes the peri-centromere regions in budding yeast (Lawrimore *et al*, 2018; Paldi *et al*, 2020). Local depletion of cohesin at centromeres in fission yeast lead to a high incidence of merotelic attachments (Bernard *et al*, 2001). A recent study revealed that vertebrate kinetochores are bipartite structures and highlighted a role for cohesin in bridging to the two parts into a functional unit (Sacristan *et al*, 2024). Lastly, enhanced cohesin binding to centromeres may facilitate the correction of merotelic attachments by the Aurora B kinase. The localization of Aurora B relies on histone H3-T3 phosphorylation by Haspin whose localization to centromeres depends largely on the cohesin subunit Pds5 in fission yeast (Yamagishi *et al*, 2010; Goto *et al*, 2017).

That chromosome segregation defects increase with TORC1 activity suggests the intriguing possibility that the fidelity of chromosome segregation could be modulated by environmental cues. Chromosome segregation defects in the *mis4* mutant were most intense in the complete rich medium YES than in the synthetic medium EMM2. The use of glutamate, a nitrogen source slightly poorer than ammonia (Davie *et al*, 2015) further reduced chromosome segregation defects. Microbial species in the wild compete with each other. When nutriments are abundant, it might be preferable to divide rapidly to colonize the niche, even at the expense of individual cells. Conversely, when nutrients become scarce, survival of the species may rely more heavily on individual fitness.

Mis4 and TORC1 control the gene response to environmental changes

In a previous study we reported that *mis4-G1487D* affects the expression of genes located in subtelomeric domains (Dheur *et al*, 2011). Here we extend the study by challenging cells with various culture conditions. Several conclusions can be drawn. Very few genes were affected when cells were actively cycling in rich media, when TORC1 activity is high. The gene list was much longer upon nitrogen deprivation, when TORC1 activity is repressed, and the list of genes evolved with time spent in G0. In aggregate 337 genes were affected in *mis4-G1487D* when compared with wild-type with a strong bias towards chromosome ends and far from centromeres. Lastly, most genes misregulated in *mis4-G1487D* were misregulated in the *mip1-R401G* mutant suggesting Mis4 and Mip1 act in a same pathway. Paradoxically, the *mis4* and *mip1* mutants remained viable during G0 although a delay was noticeable upon re-entry into the cell cycle at elevated temperature. A defect in quiescence exit was previously reported when the *mis4* gene is affected and the phenotype appears strongly dependent on the allele considered (Sajiki *et al*, 2009; Suma *et al*, 2024). It must be kept in mind that *mis4* mutants were originally screened for a defect during vegetative growth. It would be interesting to screen specifically for *mis4* alleles affecting cell survival in quiescence.

Given the role of cohesin and its loader in chromosome folding, it is tempting to speculate that TORC1 might direct cohesin to generate a chromosome architecture that is competent for transcriptional response to environmental changes. If increased binding of Mis4 and cohesin at CARs does reflect extruding cohesin complexes that have reach TAD boundaries, chromosomes might be

more compacted when TORC1 is down regulated. Conversely, high TORC1 would promote the opposite. Even if this hypothesis turned out to be correct, it does not explain why regulated genes show a bias towards chromosome ends. Chromosomes in fission yeast adopt a rabl configuration in interphase (Mizuguchi *et al*, 2015). Centromeres cluster at the SPBs while telomeres cluster in a few patches at the opposing hemisphere near the nuclear periphery. These constraints generate specific chromosomal regions with distinct molecular environments. Chromosome conformation capture and the mapping of DNA binding sites of inner nuclear membrane proteins have provided evidence of functional sub-nuclear environments that correlate with gene expression activity (Steglich *et al*, 2012; Grand *et al*, 2014). The studies suggest more internal locations of actively expressed genes, and nuclear peripheral localization of poorly expressed genes. Chromosome regions containing gene clusters that are up-regulated upon nitrogen starvation re-position from the nuclear periphery to the interior (Alfredsson-Timmins *et al*, 2009). In this regard, Mis4-regulated genes tend to be lowly expressed and enriched for nitrogen responsive genes. Modifying chromosome compaction may alter the rabl configuration or generate forces that modify the properties of the inner nuclear envelope, leading to misregulated gene expression. Indeed, loss of cohesin causes an increase in inter-chromosomal contacts and a reduction in chromosomal territoriality (Mizuguchi *et al*, 2014).

Cohesin and TORC1 have been implicated with a wide range of human pathologies, including cancer (Yoon, 2020; Waldman, 2020). Rapamycin has attracted much attention for its putative ability to mimic caloric restriction, resulting in improved health and lifespan (Bjedov & Partridge, 2011). Our study raises the intriguing possibility that some effects are mediated by cohesin and its ability to remodel chromosomes in response to various extracellular signals, including nutrients.

MATERIALS AND METHODS

Strains, media and genetic techniques

General fission yeast methods, reagents and media are described in (Moreno *et al*, 1991). All strains are listed in supplementary Table 2. Experiments were carried out using YES medium unless otherwise stated. EMM-GLU is EMM2 in which NH_4Cl was replaced with 20mM glutamate. Rapamycin (Calbiochem, 4.57mg/ml stock in DMSO) was added to the culture medium to 200ng/ml. For nitrogen deprivation, cycling cells in EMM2 (~5-10^6-10^7 cells/ml) were washed three times in EMM2-N and incubated in EMM2-N at the same density. Cell cycle arrest in YES medium was achieved by shifting cycling *cdc10-129* cells (~10^7 cells/ml) at 36°C for 3.5 hours. Hydroxyurea (HU) was used to arrest cells in early S-phase. HU (12mM) was added to cycling cells in YES (~10^7/ml) and shifted to 36.5°C for 3.5 hours. All cell cycle arrests were checked by flow cytometry analysis of DNA content. The genetic screen for *mis4* suppressors was described in (Birot *et al*, 2020). The suppressors fell into four linkage groups. To identify the mutated loci, genomic DNA was extracted from one mutant from each group and from the wild-type *S. pombe* reference strain and co-hybridized to tiling arrays as described (Birot *et al*, 2020). For the *mip1* group (5 alleles) the mutated site in each strain was identified by PCR followed by DNA sequencing. Phospho-mutants were generated using the SpEDIT method (Torres-Garcia *et al*, 2020). The introduction of the desired changes was confirmed by PCR followed by DNA sequencing. Gene mapping, sequence and annotations were from Pombase (Rutherford *et al*, 2024).

Cytological techniques

DNA content was measured by flow cytometry with an Accuri C6 Flow cytometer after Sytox Green staining of ethanol-fixed cells (Knutsen *et al*, 2011). Data were presented using the FlowJo software. Indirect immunofluorescence was done as described (Birot *et al*, 2020). Cells were imaged using a Leica DMRXA microscope and a 63X objective. Measurements were made using MetaMorph software.

Live cell analysis was performed in an imaging chamber (CoverWell PCI-2.5, Grace Bio-Labs, Bend, OR) filled with 1 ml of 1% agarose in minimal medium and sealed with a 22 × 22-mm glass coverslip. Time-lapse images of Z stacks (maximum five stacks of 0.5 µm steps, to avoid photobleaching) were taken at 60 sec intervals. Images were acquired with a CCD Retiga R6 camera (QImaging) fitted to a DM6B upright microscope with a x63 objective, using MetaMorph as a software. Intensity adjustments were made using the MetaMorph, Image J, and Adobe Photoshop packages (Adobe Systems France, Paris, France). To determine the percentage of mispositioned spindles, cells were fixed in 3.7% formaldehyde for 6 min at room temperature, washed twice in PBS, and observed in the presence of DAPI/calcofluor.

The position of the SPBs, kinetochores and centromeres were determined by visualization of the Cdc11–GFP, Ndc80–GFP and Mis6-RFP signals. Maximum intensity projections were prepared for each time point, with the images from each channel being combined into a single RGB image. These images were cropped around the cell of interest, and optional contrast enhancement was performed in MetaMorph, Image J or Photoshop where necessary. The cropped images were exported as 8-bit RGB-stacked TIFF files, with each frame corresponding to one image of the time-lapse series. For all channels, custom peak detection was performed. The successive positions of the SPBs and kinetochores/centromeres were determined.

Antibodies, protein extracts, immunoprecipitation, western blotting, phosphatase treatment, chromatin immunoprecipitation (ChIP)

Rabbit polyclonal antibodies against Rad21, Psm1, Psm3, Psm3-K106Ac, Rad21-T262 have been described previously (Feytout *et al*, 2011; Dheur *et al*, 2011; Birot *et al*, 2020). The mouse monoclonal anti-tubulin antibody TAT1 is from (Woods *et al*, 1989). Anti-Psm1-S1022p and anti-Mis4-S183p antibodies were raised by Biotem (Apprieu, France). Rabbits were immunized with the KLH-coupled peptides. Sera were immune-depleted by affinity with the non-phosphorylated form of the peptide and antibodies were affinity purified against the phosphorylated peptide. Other antibodies were of commercial source. Rabbit polyclonal anti-GFP A11122 (Molecular Probes), mouse monoclonal anti-GFP (Roche), anti-PK antibodies (monoclonal mouse anti V5 tag, AbD serotec), mouse monoclonal anti-FLAG (Sigma) and mouse monoclonal anti-myc (Santa-Cruz). For the detection of Psk1 (Thr-415) phosphorylation, protein extracts were prepared by the TCA method and western blots probed with the anti-phospho-p70 S6K antibody (cat. no. 9206, Cell Signaling Technology) as described (Morozumi et al, 2021). Protein extracts, immunoprecipitation (IP), cell fractionation and western blotting were as described (Birot *et al*, 2020). For quantitative western blot analyses, signals were captured with the ChemiDoc MP Imaging System and quantified using the Image Lab software. On beads phosphatase treatment of Mis4-GFP was done as described (Birot *et al*, 2017). Chromatin Immunoprecipitation (ChIP) was as described (Birot *et al*, 2020) using anti-FLAG, anti-GFP (A11122) and anti-Rad21 antibodies.

RNA sequencing

Total RNA from biological triplicate samples was subjected to quality control with Agilent Tapestation according to the manufacturer's instructions. To construct libraries suitable for Illumina sequencing, rRNA was depleted using the Ribominus kit (Thermo Fisher) starting with 2000 ng total RNA and then

followed by the Illumina stranded ligation sample preparation protocol starting with 100 ng rRNA depleted RNA. The protocol includes fragmentation, denaturation of RNA, cDNA synthesis, ligation of adapters, and amplification of indexed libraries. The yield and quality of the amplified libraries were analyzed using Qubit (Thermo Fisher) and the quality of the libraries was checked by using the Agilent Tapestation. The indexed cDNA libraries were normalized and combined, and the pools were sequenced on the Illumina Nextseq 2000 machine using a P3 100 cycle sequencing run, producing a sequencing length of 58 base paired end reads with dual index.

RNA-Seq Data processing and analysis

Bcl files were converted and demultiplexed to fastq using the bcl2fastq v2.20.0.422 program. STAR 2.7.10a (Dobin *et al*, 2013) was used to index the *S. pombe* reference genome (ASM294v2) and align the resulting fastq files. Mapped reads were then counted in annotated exons using featureCounts v1.5.1 (Liao *et al*, 2014). The gene annotations (Schizosaccharomyces_pombe.ASM294v2.35.gff3) and reference genome were obtained from Ensembl Fungi. The count table from featureCounts was imported into R/Bioconductor and differential gene expression was performed using the EdgeR (Robinson *et al*, 2010) package and its general linear models pipeline. For the gene expression analysis genes with no or very low expression were filtered out using the filterByExpr function and subsequently normalized using TMM normalization. Genes with an FDR adjusted p value < 0.05 were termed significantly regulated. Venn diagrams were generated using jvenn (Bardou *et al*, 2014).

Mass spectrometry

Sample preparation and protein digestion. Protein samples were solubilized in Laemmli buffer and proteins were deposited onto SDS-PAGE gel. After colloidal blue staining, each lane was cut out from the gel and was subsequently cut in 1 mm x 1 mm gel pieces. Gel pieces were destained in 25 mM ammonium bicarbonate 50% ACN, rinsed twice in ultrapure water and shrunk in ACN for 10 min. After ACN removal, gel pieces were dried at room temperature, covered with the trypsin solution (10 ng/µl in 50 mM NH4HCO3), rehydrated at 4°C for 10 min, and finally incubated overnight at 37°C. Spots were then incubated for 15 min in 50 mM NH4HCO3 at room temperature with rotary shaking. The supernatant was collected, and an H2O/ACN/HCOOH (47.5:47.5:5) extraction solution was added onto gel slices for 15 min. The extraction step was repeated twice. Supernatants were pooled and dried in a vacuum centrifuge. Digests were finally solubilized in 0.1% HCOOH.

nLC-MS/MS analysis and Label-Free Quantitative Data Analysis. Peptide mixture was analyzed on a Ultimate 3000 nanoLC system (Dionex, Amsterdam, The Netherlands) coupled to a Electrospray Orbitrap Fusion™ Lumos™ Tribrid™ Mass Spectrometer (Thermo Fisher Scientific, San Jose, CA). Ten microliters of peptide digests were loaded onto a 300-µm-inner diameter x 5-mm C18 PepMapTM trap column (LC Packings) at a flow rate of 10 µL/min. The peptides were eluted from the trap column onto an analytical 75-mm id x 50-cm C18 Pep-Map column (LC Packings) with a 5–27.5% linear gradient of solvent B in 105 min (solvent A was 0.1% formic acid and solvent B was 0.1% formic acid in 80% ACN) followed by a 10 min gradient from 27.5% to 40% solvent B. The separation flow rate was set at 300 nL/min. The mass spectrometer operated in positive ion mode at a 2-kV needle voltage. Data were acquired using Xcalibur software in a data-dependent mode. MS scans (m/z 375-1500) were recorded in the Orbitrap at a resolution of R = 120 000 (@ m/z 200) and an AGC target of 4 x 105 ions collected within 50 ms. Dynamic exclusion was set to 60 s and top speed fragmentation in HCD mode was performed over a 3 s cycle. MS/MS scans were collected in the Orbitrap with a resolution if 30,000 and maximum fill time of 54 ms. Only +2 to +7 charged ions were selected for fragmentation. Other settings were as follows: no sheath nor auxiliary gas flow, heated capillary temperature, 275 °C; normalized HCD collision energy of 30%, isolation width of 1.6 m/z, AGC target

of 5 x 104 and normalized AGC target of 100%. Monoisotopic precursor selection (MIPS) was set to Peptide and an intensity threshold was set to 2.5 x 104.

Database search and results processing. Data were searched by SEQUEST and BYONIC through Proteome Discoverer 2.5 (Thermo Fisher Scientific Inc.) against an Schizosaccharomyces pombe uniprot database (5,098 entries in v2021-01). Spectra from peptides higher than 5000 Da or lower than 350 Da were rejected. Precursor Detector node was included. Search parameters were as follows: mass accuracy of the monoisotopic peptide precursor and peptide fragments was set to 10 ppm and 0.02 Da respectively. Only b- and y-ions were considered for mass calculation. Sequest HT was used as the search algorithm : Oxidation of methionines (+16 Da), methionine loss (-131 Da), methionine loss with acetylation (-89 Da), protein N-terminal acetylation (+42 Da) and phosphorylation of Serine, Threonine and Tyrosine (+80 Da) were considered as variable modifications while carbamidomethylation of cysteines (+57 Da) was considered as fixed modification. Two missed trypsin cleavages were allowed. Peptide validation was performed using Percolator algorithm (Kall *et al*, 2007) and only "high confidence" peptides were retained corresponding to a 1% False Positive Rate at peptide level. Peaks were detected and integrated using the Minora algorithm embedded in Proteome Discoverer. Normalization was performed based on total peptide amount. Protein ratios were calculated as the median of all possible pairwise peptide ratios. A t-test was calculated based on background population of peptides or proteins. Quantitative data were considered at peptide level.

Data Availability

AKNOWLEDGMENTS

We would like to thank Tomoyuki Fukuda, Yuichi Morozumi, Janni Petersen, Kazuhiro Shiozaki, Ronit Weisman, Mitsuhiro Yanagida and the National BioResource Project for providing *S. pombe* strains and advices. Keith Gull for the gift of anti-tubulin antibodies. This work was supported by the Centre National de la Recherche Scientifique, l'Université de Bordeaux, la Région Aquitaine, la Fondation ARC pour la recherche contre le cancer (ARCPJA2021060003810) and La Ligue contre le Cancer. Dorian Besson was supported by the International Doctorate Program – IdEx University of Bordeaux and a fellowship from the Fondation ARC. Adele Marston is funded through a Wellcome Investigator Award [220780] and the Wellcome Discovery Research Platform for Hidden Cell Biology [226791]. Work in the Karl Ekwall laboratory was financed by the Swedish research council (VR-MH) and the Swedish Cancer Society (CF). We also would like to thank BEA, The core facility for Bioinformatics and Expression Analysis, which is supported by the board of research at the Karolinska Institutet and the research committee at the Karolinska hospital.

BIBLIOGRAPHY

Alfredsson-Timmins J, Kristell C, Henningson F, Lyckman S & Bjerling P (2009) Reorganization of chromatin is an early response to nitrogen starvation in Schizosaccharomyces pombe. *Chromosoma* 118: 99–112

Bardou P, Mariette J, Escudié F, Djemiel C & Klopp C (2014) jvenn: an interactive Venn diagram viewer. *BMC Bioinformatics* 15: 293

Beli P, Lukashchuk N, Wagner SA, Weinert BT, Olsen JV, Baskcomb L, Mann M, Jackson SP & Choudhary C (2012) Proteomic Investigations Reveal a Role for RNA Processing Factor THRAP3 in the DNA Damage Response. *Molecular Cell* 46: 212–225

Bernard P, Drogat J, Maure J-F, Dheur S, Vaur S, Genier S & Javerzat J-P (2006) A screen for cohesion mutants uncovers Ssl3, the fission yeast counterpart of the cohesin loading factor Scc4. *Curr Biol* 16: 875–881

Bernard P, Maure JF, Partridge JF, Genier S, Javerzat JP & Allshire RC (2001) Requirement of heterochromatin for cohesion at centromeres. *Science* 294: 2539–2542

Birot A, Eguienta K, Vazquez S, Claverol S, Bonneu M, Ekwall K, Javerzat J-P & Vaur S (2017) A second Wpl1 anti-cohesion pathway requires dephosphorylation of fission yeast kleisin Rad21 by PP4. *EMBO J* 36: 1364–1378

Birot A, Tormos-Pérez M, Vaur S, Feytout A, Jaegy J, Alonso Gil D, Vazquez S, Ekwall K & Javerzat J-P (2020) The CDK Pef1 and protein phosphatase 4 oppose each other for regulating cohesin binding to fission yeast chromosomes. *Elife* 9

Bitton DA, Schubert F, Dey S, Okoniewski M, Smith GC, Khadayate S, Pancaldi V, Wood V & Bähler J (2015) AnGeLi: A Tool for the Analysis of Gene Lists from Fission Yeast. *Front Genet* 6: 330

Bjedov I & Partridge L (2011) A longer and healthier life with TOR down-regulation: genetics and drugs. *Biochemical Society Transactions* 39: 460–465

Carlson CR, Grallert B, Stokke T & Boye E (1999) Regulation of the start of DNA replication in Schizosaccharomyces pombe. *J Cell Sci* 112 (Pt 6): 939–46

Chao WC, Murayama Y, Munoz S, Costa A, Uhlmann F & Singleton MR (2015) Structural Studies Reveal the Functional Modularity of the Scc2-Scc4 Cohesin Loader. *Cell Rep* 12: 719–25

Chia KH, Fukuda T, Sofyantoro F, Matsuda T, Amai T & Shiozaki K (2017) Ragulator and GATOR1 complexes promote fission yeast growth by attenuating TOR complex 1 through Rag GTPases. *eLife* 6

Christensen GL, Kelstrup CD, Lyngsø C, Sarwar U, Bøgebo R, Sheikh SP, Gammeltoft S, Olsen JV & Hansen JL (2010) Quantitative phosphoproteomics dissection of seven-transmembrane receptor signaling using full and biased agonists. *Mol Cell Proteomics* 9: 1540–1553

Ciosk R, Shirayama M, Shevchenko A, Tanaka T, Toth A & Nasmyth K (2000) Cohesin's binding to chromosomes depends on a separate complex consisting of Scc2 and Scc4 proteins. *Mol Cell* 5: 243–254

Collier JE, Lee BG, Roig MB, Yatskevich S, Petela NJ, Metson J, Voulgaris M, Gonzalez Llamazares A, Lowe J & Nasmyth KA (2020) Transport of DNA within cohesin involves clamping on top of engaged heads by Scc2 and entrapment within the ring by Scc3. *eLife* 9

Costantino L, Hsieh TS, Lamothe R, Darzacq X & Koshland D (2020) Cohesin residency determines chromatin loop patterns. *eLife* 9

Courtheoux T, Gay G, Gachet Y & Tournier S (2009) Ase1/Prc1-dependent spindle elongation corrects merotely during anaphase in fission yeast. *J Cell Biol* 187: 399–412

Davidson IF, Bauer B, Goetz D, Tang W, Wutz G & Peters JM (2019) DNA loop extrusion by human cohesin. *Science*

Davidson IF & Peters J-M (2021) Genome folding through loop extrusion by SMC complexes. *Nat Rev Mol Cell Biol* 22: 445–464

Davie E, Forte GMA & Petersen J (2015) Nitrogen regulates AMPK to control TORC1 signaling. *Curr Biol* 25: 445–454

Dephoure N, Zhou C, Villén J, Beausoleil SA, Bakalarski CE, Elledge SJ & Gygi SP (2008) A quantitative atlas of mitotic phosphorylation. *Proc Natl Acad Sci U S A* 105: 10762–10767

Dheur S, Saupe SJ, Genier S, Vazquez S & Javerzat J-P (2011) Role for cohesin in the formation of a heterochromatic domain at fission yeast subtelomeres. *Mol Cell Biol* 31: 1088–1097

Dobin A, Davis CA, Schlesinger F, Drenkow J, Zaleski C, Jha S, Batut P, Chaisson M & Gingeras TR (2013) STAR: ultrafast universal RNA-seq aligner. *Bioinformatics* 29: 15–21

Feytout A, Vaur S, Genier S, Vazquez S & Javerzat J-P (2011) Psm3 acetylation on conserved lysine residues is dispensable for viability in fission yeast but contributes to Eso1-mediated sister chromatid cohesion by antagonizing Wpl1. *Mol Cell Biol* 31: 1771–1786

Fukuda T & Shiozaki K (2018) The Rag GTPase-Ragulator complex attenuates TOR complex 1 signaling in fission yeast. *Autophagy* 14: 1105–1106

Fukuda T, Sofyantoro F, Tai YT, Chia KH, Matsuda T, Murase T, Morozumi Y, Tatebe H, Kanki T & Shiozaki K (2021) Tripartite suppression of fission yeast TORC1 signaling by the GATOR1-Sea3 complex, the TSC complex, and Gcn2 kinase. *eLife* 10

Furuya K, Takahashi K & Yanagida M (1998) Faithful anaphase is ensured by Mis4, a sister chromatid cohesion molecule required in S phase and not destroyed in G1 phase. *Genes Dev* 12: 3408–3418

González A & Hall MN (2017) Nutrient sensing and TOR signaling in yeast and mammals. *EMBO J* 36: 397–408

Goto Y, Yamagishi Y, Shintomi-Kawamura M, Abe M, Tanno Y & Watanabe Y (2017) Pds5 Regulates Sister-Chromatid Cohesion and Chromosome Bi-orientation through a Conserved Protein Interaction Module. *Current Biology* 27: 1005–1012

Grand RS, Pichugina T, Gehlen LR, Jones MB, Tsai P, Allison JR, Martienssen R & O'Sullivan JM (2014) Chromosome conformation maps in fission yeast reveal cell cycle dependent sub nuclear structure. *Nucleic Acids Research* 42: 12585–12599

Gregan J, Polakova S, Zhang L, Tolic-Norrelykke IM & Cimini D (2011) Merotelic kinetochore attachment: causes and effects. *Trends Cell Biol* 21: 374–81

Halova L, Cobley D, Franz-Wachtel M, Wang T, Morrison KR, Krug K, Nalpas N, Maček B, Hagan IM, Humphrey SJ, *et al* (2021) A TOR (target of rapamycin) and nutritional phosphoproteome of fission yeast reveals novel targets in networks conserved in humans. *Open Biol* 11: 200405

Hayashi T, Hatanaka M, Nagao K, Nakaseko Y, Kanoh J, Kokubu A, Ebe M & Yanagida M (2007) Rapamycin sensitivity of the Schizosaccharomyces pombe tor2 mutant and organization of

two highly phosphorylated TOR complexes by specific and common subunits. *Genes Cells* 12: 1357–70

Hirai H, Sen Y, Tamura M & Ohta K (2023) TOR inactivation triggers heterochromatin formation in rDNA during glucose starvation. *Cell Reports* 42

Hu B, Petela N, Kurze A, Chan KL, Chapard C & Nasmyth K (2015) Biological chromodynamics: a general method for measuring protein occupancy across the genome by calibrating ChIP-seq. *Nucleic Acids Res* 43: e132

Ikai N, Nakazawa N, Hayashi T & Yanagida M (2011) The reverse, but coordinated, roles of Tor2 (TORC1) and Tor1 (TORC2) kinases for growth, cell cycle and separase-mediated mitosis in Schizosaccharomyces pombe. *Open Biology* 1: 110007

Kagami A, Sakuno T, Yamagishi Y, Ishiguro T, Tsukahara T, Shirahige K, Tanaka K & Watanabe Y (2011) Acetylation regulates monopolar attachment at multiple levels during meiosis I in fission yeast. *EMBO Rep* 12: 1189–95

Kall L, Canterbury JD, Weston J, Noble WS & MacCoss MJ (2007) Semi-supervised learning for peptide identification from shotgun proteomics datasets. *Nature methods* 4: 923–5

Kettenbach AN, Deng L, Wu Y, Baldissard S, Adamo ME, Gerber SA & Moseley JB (2015) Quantitative phosphoproteomics reveals pathways for coordination of cell growth and division by the conserved fission yeast kinase pom1. *Mol Cell Proteomics* 14: 1275–87

Knutsen JH, Rein ID, Rothe C, Stokke T, Grallert B & Boye E (2011) Cell-cycle analysis of fission yeast cells by flow cytometry. *PLoS One* 6: e17175

Laribee RN & Weisman R (2020) Nuclear Functions of TOR: Impact on Transcription and the Epigenome. *Genes* 11

Lawrimore J, Doshi A, Friedman B, Yeh E & Bloom K (2018) Geometric partitioning of cohesin and condensin is a consequence of chromatin loops. *MBoC* 29: 2737–2750

Lengronne A, Katou Y, Mori S, Yokobayashi S, Kelly GP, Itoh T, Watanabe Y, Shirahige K & Uhlmann F (2004) Cohesin relocation from sites of chromosomal loading to places of convergent transcription. *Nature* 430: 573–8

Liao Y, Smyth GK & Shi W (2014) featureCounts: an efficient general purpose program for assigning sequence reads to genomic features. *Bioinformatics* 30: 923–930

Matsuda S, Kikkawa U, Uda H & Nakashima A (2020) S. pombe Pef1/CDK5 regulates sexual differentiation through control of the TORC1 pathway and autophagy. *J Cell Sci*

Mayya V, Lundgren DH, Hwang S-I, Rezaul K, Wu L, Eng JK, Rodionov V & Han DK (2009) Quantitative phosphoproteomic analysis of T cell receptor signaling reveals system-wide modulation of protein-protein interactions. *Sci Signal* 2: ra46

Mizuguchi T, Barrowman J & Grewal SIS (2015) Chromosome domain architecture and dynamic organization of the fission yeast genome. *FEBS Lett* 589: 2975–2986

Mizuguchi T, Fudenberg G, Mehta S, Belton JM, Taneja N, Folco HD, FitzGerald P, Dekker J, Mirny L, Barrowman J, *et al* (2014) Cohesin-dependent globules and heterochromatin shape 3D genome architecture in S. pombe. *Nature* 516: 432–435

Molnar M, Doll E, Yamamoto A, Hiraoka Y & Kohli J (2003) Linear element formation and their role in meiotic sister chromatid cohesion and chromosome pairing. *J Cell Sci* 116: 1719–1731

Moreno S, Klar A & Nurse P (1991) Molecular genetic analysis of fission yeast Schizosaccharomyces pombe. *Methods Enzymol* 194: 795–823

Morozumi Y, Hishinuma A, Furusawa S, Sofyantoro F, Tatebe H & Shiozaki K (2021) Fission yeast TOR complex 1 phosphorylates Psk1 through an evolutionarily conserved interaction mediated by the TOS motif. *J Cell Sci* 134

Murayama Y, Samora CP, Kurokawa Y, Iwasaki H & Uhlmann F (2018) Establishment of DNA-DNA Interactions by the Cohesin Ring. *Cell* 172: 465-477 e15

Murayama Y & Uhlmann F (2015) DNA Entry into and Exit out of the Cohesin Ring by an Interlocking Gate Mechanism. *Cell* 163: 1628–40

Nakashima A, Otsubo Y, Yamashita A, Sato T, Yamamoto M & Tamanoi F (2012) Psk1, an AGC kinase family member in fission yeast, is directly phosphorylated and controlled by TORC1 and functions as S6 kinase. *J Cell Sci* 125: 5840–5849

Oldenkamp R & Rowland BD (2022) A walk through the SMC cycle: From catching DNAs to shaping the genome. *Mol Cell* 82: 1616–1630

Otsubo Y, Nakashima A, Yamamoto M & Yamashita A (2017) TORC1-Dependent Phosphorylation Targets in Fission Yeast. *Biomolecules* 7: 50

Paldi F, Alver B, Robertson D, Schalbetter SA, Kerr A, Kelly DA, Baxter J, Neale MJ & Marston AL (2020) Convergent genes shape budding yeast pericentromeres. *Nature* 582: 119–123

Pan C, Olsen JV, Daub H & Mann M (2009) Global Effects of Kinase Inhibitors on Signaling Networks Revealed by Quantitative Phosphoproteomics*. *Molecular & Cellular Proteomics* 8: 2796–2808

Park DS, Nguyen SC, Isenhart R, Shah PP, Kim W, Barnett RJ, Chandra A, Luppino JM, Harke J, Wai M, *et al* (2023) High-throughput Oligopaint screen identifies druggable 3D genome regulators. *Nature* 620: 209–217

Pidoux AL, Uzawa S, Perry PE, Cande WZ & Allshire RC (2000) Live analysis of lagging chromosomes during anaphase and their effect on spindle elongation rate in fission yeast. *J Cell Sci* 113 Pt 23: 4177-4191.

Reidman S, Cohen A, Kupiec M & Weisman R (2019) The cytosolic form of aspartate aminotransferase is required for full activation of TOR complex 1 in fission yeast. *J Biol Chem* 294: 18244–18255

Rigbolt KTG, Prokhorova TA, Akimov V, Henningsen J, Johansen PT, Kratchmarova I, Kassem M, Mann M, Olsen JV & Blagoev B (2011) System-wide temporal characterization of the proteome and phosphoproteome of human embryonic stem cell differentiation. *Sci Signal* 4: rs3

Robinson MD, McCarthy DJ & Smyth GK (2010) edgeR: a Bioconductor package for differential expression analysis of digital gene expression data. *Bioinformatics* 26: 139–140

Ruse CI, McClatchy DB, Lu B, Cociorva D, Motoyama A, Park SK & Yates JR (2008) Motif-specific sampling of phosphoproteomes. *J Proteome Res* 7: 2140–2150

Rutherford KM, Lera-Ramírez M & Wood V (2024) PomBase: a Global Core Biodata Resource-growth, collaboration, and sustainability. *Genetics* 227: iyae007

Sacristan C, Samejima K, Ruiz LA, Deb M, Lambers MLA, Buckle A, Brackley CA, Robertson D, Hori T, Webb S, *et al* (2024) Vertebrate centromeres in mitosis are functionally bipartite structures stabilized by cohesin. *Cell* 0

Sajiki K, Hatanaka M, Nakamura T, Takeda K, Shimanuki M, Yoshida T, Hanyu Y, Hayashi T, Nakaseko Y & Yanagida M (2009) Genetic control of cellular quiescence in S. pombe. *J Cell Sci* 122: 1418–29

Sajiki K, Tahara Y, Villar-Briones A, Pluskal T, Teruya T, Mori A, Hatanaka M, Ebe M, Nakamura T, Aoki K, *et al* (2018) Genetic defects in SAPK signalling, chromatin regulation, vesicle transport and CoA-related lipid metabolism are rescued by rapamycin in fission yeast. *Open Biol* 8: 170261

Schmidt CK, Brookes N & Uhlmann F (2009) Conserved features of cohesin binding along fission yeast chromosomes. *Genome Biol* 10: R52

Shi Z, Gao H, Bai XC & Yu H (2020) Cryo-EM structure of the human cohesin-NIPBL-DNA complex. *Science* 368: 1454–1459

van Slegtenhorst M, Carr E, Stoyanova R, Kruger WD & Henske EP (2004) Tsc1+ and tsc2+ regulate arginine uptake and metabolism in Schizosaccharomyces pombe. *J Biol Chem* 279: 12706–12713

Steglich B, Filion GJ, van Steensel B & Ekwall K (2012) The inner nuclear membrane proteins Man1 and Ima1 link to two different types of chromatin at the nuclear periphery in S. pombe. *Nucleus* 3: 77–87

Suma M, Arakawa O, Tahara Y, Sajiki K, Saitoh S & Yanagida M (2024) In quiescent G0 phase, Schizosaccharomyces pombe Mis4 ensures full nuclear separation during the subsequent M phase. 2024.03.29.587322 doi:10.1101/2024.03.29.587322 [PREPRINT]

Swaffer MP, Jones AW, Flynn HR, Snijders AP & Nurse P (2018) Quantitative Phosphoproteomics Reveals the Signaling Dynamics of Cell-Cycle Kinases in the Fission Yeast Schizosaccharomyces pombe. *Cell Rep* 24: 503–514

Tay YD, Leda M, Spanos C, Rappsilber J, Goryachev AB & Sawin KE (2019) Fission Yeast NDR/LATS Kinase Orb6 Regulates Exocytosis via Phosphorylation of the Exocyst Complex. *Cell Rep* 26: 1654-1667 e7

Torres-Garcia S, Di Pompeo L, Eivers L, Gaborieau B, White SA, Pidoux AL, Kanigowska P, Yaseen I, Cai Y & Allshire RC (2020) SpEDIT: A fast and efficient CRISPR/Cas9 method for fission yeast. *Wellcome open research* 5: 274

Vaur S, Feytout A, Vazquez S & Javerzat J-P (2012) Pds5 promotes cohesin acetylation and stable cohesin-chromosome interaction. *EMBO Rep* 13: 645–652

Waldman T (2020) Emerging themes in cohesin cancer biology. *Nature reviews Cancer* 20: 504–515

Wei Y, Lee NN, Pan L, Dhakshnamoorthy J, Sun LL, Zofall M, Wheeler D & Grewal SIS (2021) TOR targets an RNA processing network to regulate facultative heterochromatin, developmental gene expression and cell proliferation. *Nat Cell Biol* 23: 243–256

Woods A, Sherwin T, Sasse R, MacRae TH, Baines AJ & Gull K (1989) Definition of individual components within the cytoskeleton of Trypanosoma brucei by a library of monoclonal antibodies. *J Cell Sci* 93: 491–500

Xu B, Lee KK, Zhang L & Gerton JL (2013) Stimulation of mTORC1 with L-leucine rescues defects associated with Roberts syndrome. *PLoS Genet* 9: e1003857

Yamagishi Y, Honda T, Tanno Y & Watanabe Y (2010) Two Histone Marks Establish the Inner Centromere and Chromosome Bi-Orientation. *Science* 330: 239–243

Yoon MS (2020) Nanotechnology-Based Targeting of mTOR Signaling in Cancer. *International journal of nanomedicine* 15: 5767–5781

Zahedi Y, Zeng S & Ekwall K (2023) An essential role for the Ino80 chromatin remodeling complex in regulation of gene expression during cellular quiescence. *Chromosome Res* 31: 14

Zhao T, Fan J, Abu-Zaid A, Burley SK & Zheng XFS (2024) Nuclear mTOR Signaling Orchestrates Transcriptional Programs Underlying Cellular Growth and Metabolism. *Cells* 13: 781

Zheng H & Xie W (2019) The role of 3D genome organization in development and cell differentiation. *Nature reviews Molecular cell biology* 20: 535–550

Zhou H, Zheng L, Lu K, Gao Y, Guo L, Xu W & Wang X (2017) Downregulation of Cohesin Loading Factor Nipped-B-Like Protein (NIPBL) Induces Cell Cycle Arrest, Apoptosis, and Autophagy of Breast Cancer Cell Lines. *Med Sci Monit* 23: 4817–4825

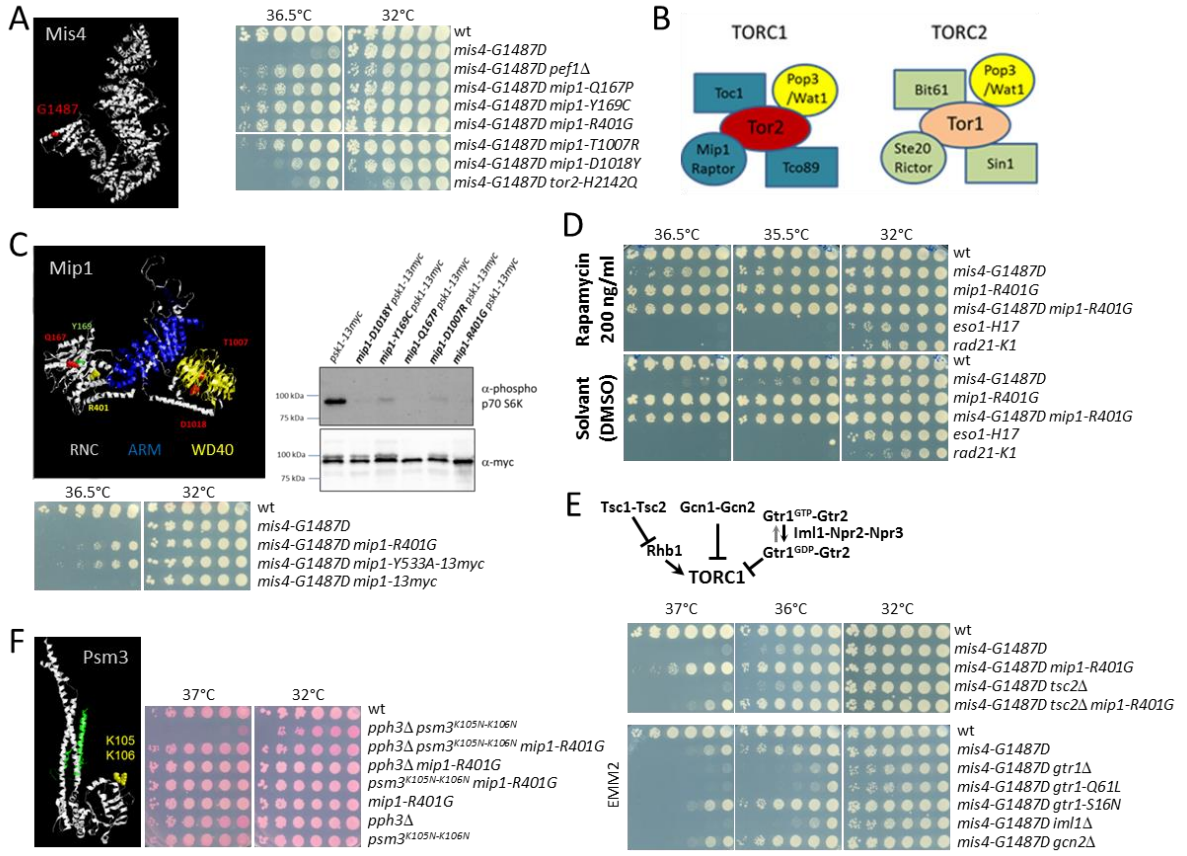

Figure 1. Genetic evidence linking TORC1 to cohesin. (A) Model structure of Mis4. The G1487D substitution confers a thermosensitive growth (Ts) phenotype. The cell growth assay shows the suppression of the Ts phenotype by the indicated mutations. **(B)** Composition of fission yeast TORC complexes (adapted from (Hayashi et al, 2007)). **(C-D)** Down-regulation of TORC1 suppresses the Ts growth defect of *mis4-G1487D*. (**C**) Model structure of Mip1 highlighting amino-acid substitutions in the suppressor mutants (RNC :Raptor N-terminal CASPase-like domain, ARM: Armadillo-type fold, WD40: WD-40 repeats). All *mip1* mutant alleles from the genetic screen showed reduced phosphorylation of the S6-kinase Psk1, a known TORC1 substrate. Conversely, *mip1-Y533A* which is deficient for Psk1 binding and phosphorylation, suppressed the Ts phenotype of *mis4-G1487D.* (**D**) The TORC1 inhibitor rapamycin rescued *mis4-G1487D* but not *eso1* and *rad21* mutants. **(E)** Genetic upregulation of TORC1 exacerbates the Ts phenotype of *mis4-G1487D*. The deletion of *gcn2* or *tsc2* was essentially neutral, although the suppression by *mip1-R401G* was reduced in a *tsc2* deleted background. Deletion of *gtr1, iml1* or *gtr1-Q61L* mimicking the GTP-bound, inactive state of GATOR exacerbated the Ts phenotype of *mis4-G1487D* while mimicking the active GDP-bound form (*gtr1-16N*) was neutral. (**F**) Psm3$^{K105N-K106N}$ confers a Ts phenotype when combined with the deletion of *pph3*, encoding the catalytic subunit of PP4, a phenotype efficiently rescued by *mip1-R401G*.

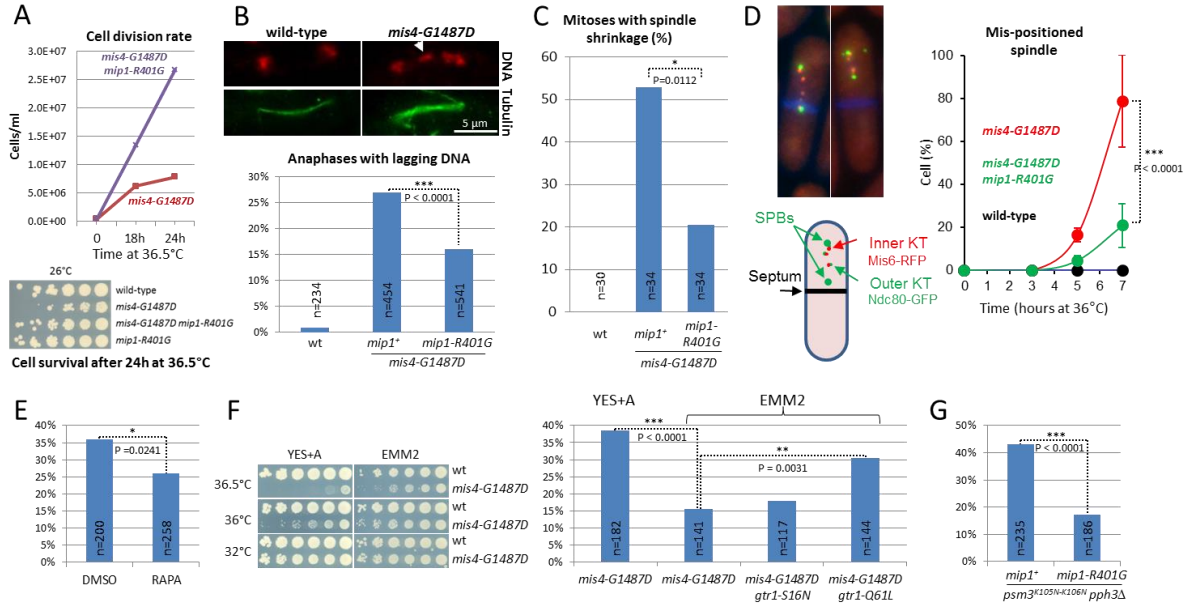

Figure 2. The incidence of chromosome segregation defects in *mis4-G1487D* is modulated by TORC1. (A) Exponential growing cells at 25°C were shifted at 36.5°C for 24 hours. The growth curve shows that *mip1-R401G* suppressed the *mis4-G1487D* temperature growth defect. Cell survival after the 24 hours temperature shift was addressed by plating serial 5-fold cell dilutions at permissive temperature for *mis4-G1487D* ($4x10^4$ cells in the first row). Cell survival was reduced ~25 fold in *mis4-G1487D* and restored to wild-type levels when combined with *mip1-R401G*. (**B**) Exponentially growing cells at 25°C were shifted at 36°C for one doubling. DNA was stained with DAPI (red, pseudo-colour) and tubulin detected by indirect immunofluorescence (green). Lagging DNA (white arrow) was defined as DAPI-stained material on the anaphase spindle (length>5µm). (**C**) Spindle shrinkage events (shrinkage of more than 0.5µm) were detected by live analysis of cells undergoing anaphase at 36.5°C (Fig.2 supplement 2). (**D**) Anaphase cells with displaced spindle. Cells were cultured at 36.5°C, fixed and stained with Calcofluor to visualize septa. Shown are mean and SD from three independent experiments (n>65 cells per strain and per experiment). (**E**) Rapamycin reduces the incidence of anaphases with lagging DNA. Rapamycin (RAPA, 200ng/ml) or solvant alone (DMSO) was added to cycling cells at 25°C and the cultures shifted to 36°C for one doubling of the cell population. Samples were treated as in B. (**F**) Left, cell growth assay showing that the Ts growth defect of *mis4-G1487D* is more severe in YES+A medium that in EMM2. Right, the frequency of anaphases with lagging DNA is higher in YES+A than in EMM2. The inactive form of the TORC1 inhibitor Gtr1 (Gtr1-Q61L) increased the frequency of abnormal anaphases while the active form was neutral (Gtr1-S16N). Cells were treated as in B. (**G**) The *mip1* mutant reduced the frequency of anaphases with lagging DNA in the *psm3*$^{K105-K106N}$ *pph3*Δ background. Cells were treated as in B. (*) (**) (***), P-values from two-sided Fisher's exact test.

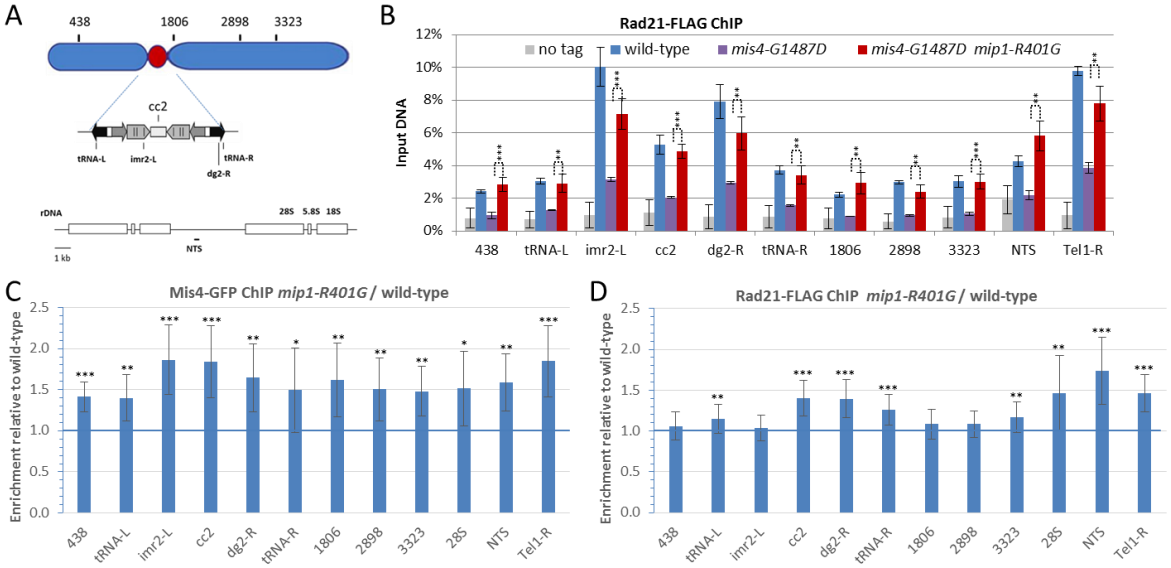

Figure 3. Increased cohesin binding to Cohesin Associated Regions in the Raptor mutant *mip1-R401G.* (A) Chromosomal sites examined were Cohesin Associated Regions along the arms (438, 1806, 2898 and 3323) and centromere of chromosome 2, the non-transcribed spacer region (NTS) of the rDNA gene cluster on chromosome 3 and the chromosome 1 right telomere. Within the centromere, the central core (*cc2*) which is the site of kinetochore assembly, the *imr* and *dg* repeats that flank the central core on either side and at tRNA rich domains that delineate the centromere. (**B**) The *mip1-R401G* mutation restores cohesin binding in *mis4-G1487D* cells. Cohesin binding to chromatin was monitored by Rad21-FLAG ChIP in G1 cells (*cdc10-129* arrest) at 36.5°C. Error bars = SD from 4 ChIPs, except for *mis4-G1487D* (3 ChIPs). ***P ≤ 0.001, **P ≤ 0.01, *P ≤ 0.05 by two-tailed, unpaired t-test with 95% confidence interval. **(C-D)** The *mip1-R401G* mutation increased Mis4 and Rad21 binding in *mis4*$^{+}$ cells. ChIP assays were made with *cdc10-129* arrested cells. (**C**) Mean and SD were calculated from 2 independent experiments and 4 technical replicates per experiment. (**D**) Mean and SD were calculated from 4 independent experiments and 4 technical replicates per experiment. ***P ≤ 0.001, **P ≤ 0.01, *P ≤ 0.05, by two-tailed, one sample t-test with 95% confidence interval.

A

	Bait = Rad21-PK			Bait = Mis4-GFP		
	Coverage [%]	# Peptides	Abundance Ratio vs no tag control	Coverage [%]	# Peptides	Abundance Ratio vs no tag control
Tor2	28	56	12.3	27	53	8.0
Mip1	5	5	7.9	9	10	3.3
Toc1	19	8	6.6	18	8	3.7
Wat1	42	10	8.4	32	8	5.1
Tco89	6	2	Abs from no tag	20	7	2.5

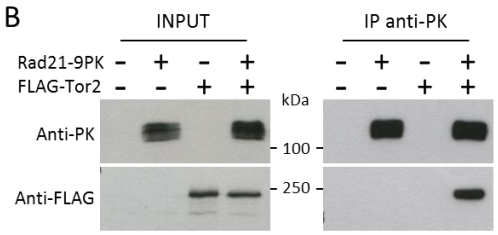

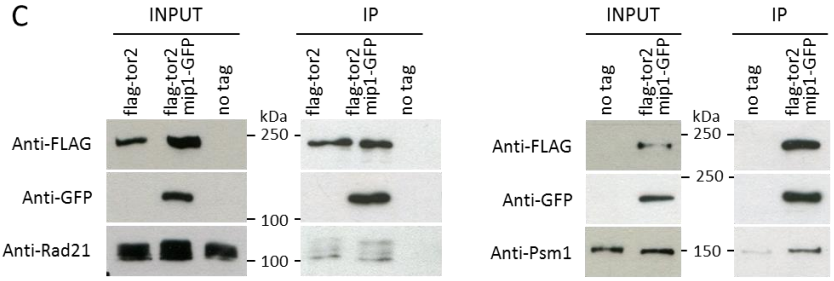

Figure 4. TORC1 components co-purify with Rad21 and Mis4. (A) Affinity purifications (triplicate samples) were made from G1 cells (*cdc10-129* arrest) and proteins analysed by label-free mass spectrometry. **(B-C)** Reciprocal co-immunoprecipitation experiments. Western blots were probed with the indicated antibodies. **(B)** Rad21-PK IP *(cdc10-129* arrested cells). **(C)** Tor2-FLAG IP (cycling cells).

A

Annotated Sequence	Modifications	Qvality PEP	# PSMs	Modifications in Master Proteins	Abundance Ratio: *mip1-R401G* / wt
[R].EYSEELDQMSPNLR.[A]	1xPhospho [S10]; 1xOxidation [M9]	6,3051E-16	11	**Psm1_O94383 1xPhospho [S1022]**	**0,553**
[R].EYSEELDQMSPNLR.[A]	1xPhospho [S10]	6,3051E-16	15	**Psm1_O94383 1xPhospho [S1022]**	**0,6**
[R].VFNAVQLCSPK.[K]	1xCarbamidomethyl [C8]; 1xPhospho [S9]	2,9719E-05	4	**Mis4_Q09725 1xPhospho [S183]**	**0,001**

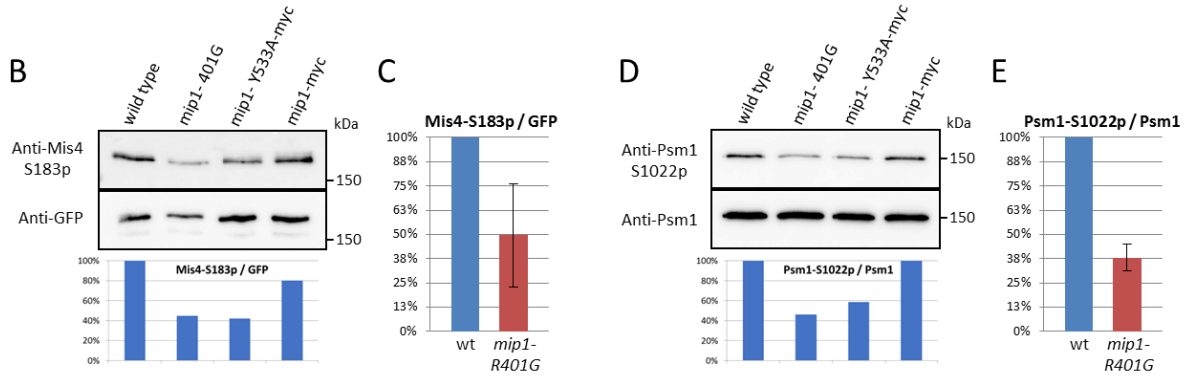

Figure 5. Reduced phosphorylation of Mis4-S183 and Psm1-S1022 in the *mip1* mutants. (A) Mis4-GFP and Cohesin (Rad21-PK) were affinity-purified from G1 cells (*cdc10-129* arrest). Triplicate samples were analyzed by label-free mass spectrometry. Mis4-S183 and Psm1-S1022 phosphorylation levels were reduced in the *mip1-R401G* background. **(B)** Mis4-GFP immunoprecipitations made from cycling cells. Western-blots were probed with anti-Mis4-S183p and anti-GFP antibodies. **(C)** Mean ratio +/- SD from three Mis4-GFP immunoprecipitations (*cdc10* arrested cells). (**D**) Rad21-FLAG immunoprecipitations made from G1 cells (*cdc10-129* arrest). Western blots were probed with anti-Psm1-S1022p and anti-Psm1 antibodies. (**E**) Mean ratio +/- SD from three experiments (*cdc10-129* arrested cells).

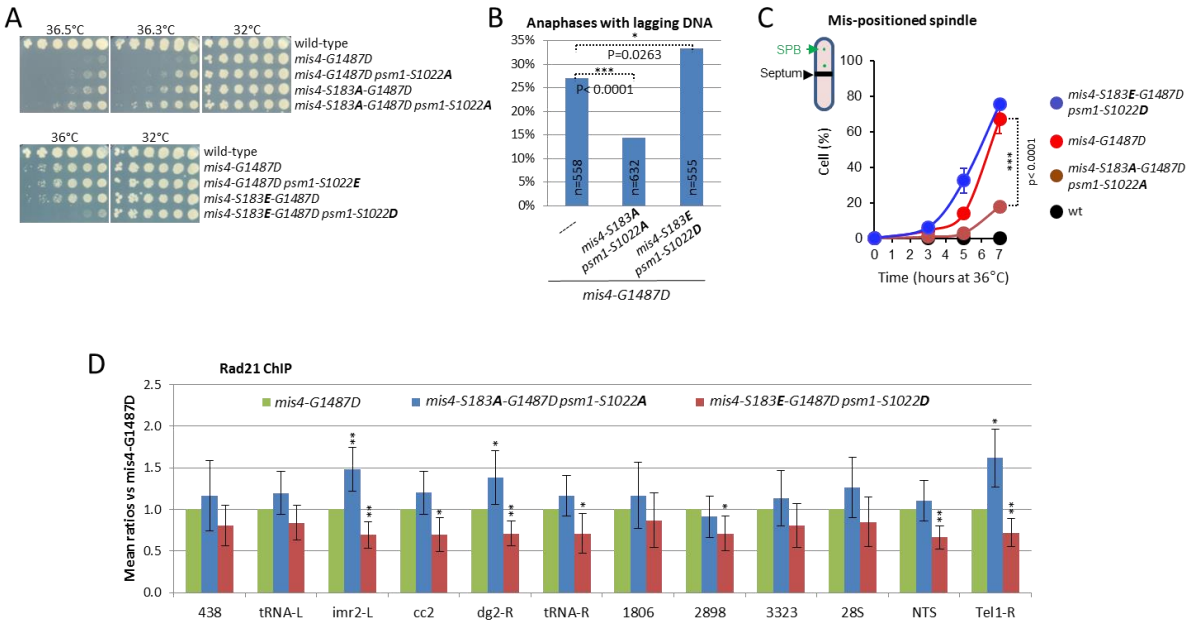

Figure 6. Mimicking the non-phosphorylated state of Psm1-S1022 and Mis4-S183 alleviates *mis4-G1487D* phenotypes while phospho-mimetics have the opposite effect. (A) Cell growth assays. (**B)** Exponentially growing cells at 25°C were shifted at 36°C for 3.5hrs (one doubling). DNA was stained with DAPI and tubulin detected by indirect immunofluorescence. Lagging DNA was defined as DAPI-stained material on the anaphase spindle (length>5µm). P-values from two-sided Fisher's exact test. (**C**) Anaphase cells with displaced spindle. Cells were cultured at 36.5°C, fixed and stained with Calcofluor to visualize septa. Mean and SD from three independent experiments (n>70 cells per strain and per experiment). P-value from two-sided Fisher's exact test. (**D**) Rad21 ChIP. Exponentially growing cells at 25°C were shifted at 36°C for 3.5hrs (one doubling). Mean and SD from 6 ratios and 2 independent experiments. **P ≤ 0.01, *P ≤ 0.05, by two-tailed, one sample t-test with 95% confidence interval.

Category_Name	GeneSet_Name	over_represented/ under_represented	Corrected pvalue
Gene Features	Abs. distance from telomere	Lower	1.99E-16
Gene Features	Relative distance from telomere	Lower	3.73E-13
Gene Features	Relative distance from centromere	Higher	3.73E-13
Gene Features	Intron-containing genes	Underrepresented	1.94E-12
Gene Features	Intron-less genes	Enriched	1.94E-12
Gene Expression	Caffeine and Rapamycin induced	Enriched	1.42E-16
Gene Expression	Late meiotic genes	Enriched	4.73E-12
Gene Expression	Reproduction module	Enriched	7.99E-10
Gene Expression	Stress module	Enriched	1.94E-09
Gene Expression	Core Environmental Stress Response induced	Enriched	4.53E-09
Gene Expression	Lowly expressed	Enriched	1.07E-08
Gene Expression	Sporulation module	Enriched	1.47E-08
Gene Expression	Meiosis sporulation module	Enriched	2.85E-05
Gene Expression	Nitrogen depletion total meiotic genes	Enriched	3.10E-05
GO Biological Process	transmembrane transport	Enriched	3.80E-05
GO Cellular Component	plasma membrane	Enriched	6.13E-05
GO Molecular Function	ion transmembrane transporter activity	Enriched	4.58E-06

Figure 7. *mis4-G1487D* affects gene response to environmental changes. RNA-sequencing (biological triplicates) was performed on cells growing in rich medium at 25°C (V25), after one cell doubling at 36.5°C (V36.5) and on G1-arrested cells (*cdc10-129*) at 36.5°C (G1_36.5). For nitrogen starvation, cells grown in EMM2 were deprived from nitrogen for 24H at 25°C (T0-N). One half of the culture was shifted to 36.5°C for 4 days (T4D36.5) while the other half was left at 25°C for 4 days (T4D25). (**A**) Number of genes misregulated in *mis4-G1487D* versus wild-type for each condition. (**B**) Proportion of misregulated genes that are specific to each experimental condition. (**C**) Overlap between genes misregulated in *mis4-G1487D* and *mip1-R401G* versus wild-type in all experimental conditions. (**D-E**) Overlap with genes upregulated in *tor2ts6* (Wei et al., 2021) and genes upregulated during G0 (Zahedi et al., 2023) (**F**) Gene features and GO-term analysis for the 337 *mis4*-regulated genes. (**G**) Browser view of *mis4*-regulated genes showing the distribution bias towards the ends of chromosomes 1 and 2.